Modeling Interactive Effects of Manganese Bioavailability, Nitrogen Deposition, and Warming on Soil Carbon Storage

Benjamin N. Sulman[1,†] (0000-0002-3265-6691) &
Elizabeth M. Herndon[1,†] (0000-0002-9194-5493)

[1] Environmental Sciences Division, Oak Ridge National Laboratory, Oak Ridge, TN 37830

Corresponding author: Elizabeth Herndon (herndonem@ornl.gov)

†Authors contributed equally to this work

Key Points:

- We developed a biogeochemical model simulating how manganese bioavailability impacts soil carbon storage in temperate forests
- Manganese redistribution to surface soils by plants enhanced decomposition and decreased carbon storage in the soil profile
- Our model predicts that low manganese bioavailability may generate nutrient limitation that decreases warming effects on decomposition

Abstract

Manganese (Mn) is a redox-active micronutrient that has been shown to accelerate plant litter decomposition; however, the effect of Mn-promoted decomposition on soil C storage is unclear. We present a novel biogeochemical model simulating how Mn bioavailability influences soil organic C (SOC) stocks in a soil profile (< 50 cm) within a temperate forest. In our model, foliar Mn increased in response to increasing soluble Mn released through Mn-oxide (birnessite) dissolution in mineral soil layers. The ensuing Mn enrichment in leaf litter redistributed Mn to the surface forest floor layer, promoted enzymatic oxidation of lignin, and decreased SOC stocks. Total SOC loss was partially mitigated by accumulation of lignin-oxidation products as mineral-associated organic C. We also explored how Mn-driven changes to C storage interacted with effects of N deposition and warming. Nitrogen enrichment inhibited Mn-dependent lignin degradation, increasing SOC stocks and weakening their dependence on Mn bioavailability. Warming stimulated decomposition and reduced C stocks but was less effective at low Mn bioavailability. Our model results suggest that SOC stocks are sensitive to Mn bioavailability because increased plant uptake redistributes Mn to surface soils where it can enhance litter decomposition. Based on our simulations, we predict that Mn becomes limiting to litter decomposition where Mn is poorly soluble. Depletion of bioavailable Mn or other cofactors that are critical to decomposition could limit the response of organic C stocks to warming over time, but quantitative projections of the role of Mn bioavailability in regulating decomposition requires additional measurements to constrain model uncertainties.

Plain Language Summary

Carbon that is removed from the atmosphere by plants and stored in soils has the potential to partially offset greenhouse gas emissions and mitigate climate change. However, predictions of soil carbon storage are challenged by limited understanding of complex interactions between biological and geochemical processes that influence how quickly organic matter decomposes in the soil. We developed a novel model that simulates how cycling of the micronutrient manganese between soils and plants impacts carbon storage in a soil profile. Although it has been demonstrated that manganese is involved in breakdown of lignin, an important component of plant litter, its effects on soil carbon storage are unknown. We also explore how effects of manganese interact with two other major global perturbations: warming and nitrogen deposition to soils. From our model results, we determine that high levels of manganese uptake by plants ultimately generate manganese-rich surface soils that promote litter decomposition and decrease soil carbon storage. Nitrogen deposition increased carbon storage by inhibiting effects of manganese on decomposition. Decomposition increased with warming but was inhibited by low manganese bioavailability. Our model provides a novel framework for simulating how soil properties that control micronutrient availability to plants can impact soil carbon dynamics.

1 Introduction

Changes in soil C stocks driven by climate change, nitrogen deposition, and other global change factors as well as temporal changes driven by plant-soil interactions are important uncertainties in projections of the global C cycle (Ciais et al., 2013). Current terrestrial C cycle models generally simulate soil organic matter (SOM) decomposition rates using simple, empirical approaches that depend only on the properties of specific SOM pools (e.g., litter quality) and a limited set of climatic and soil factors (e.g., temperature, moisture, and nutrient constraints) (Todd-Brown et al., 2013). However, the response of soil respiration to warming is highly dependent on soil parameters that vary across and within biomes (Haaf, Six, & Doetterl, 2021). Many biogeochemical and land surface models, including the widely used CENTURY model, parameterize litter quality as a function of decomposition-resistant lignin pools (Parton, 1998; Ricciuto, Sargsyan, & Thornton, 2018; Zaehle et al., 2014). While some soil organic C (SOC) models are beginning to incorporate microbiology, interactions with macronutrients, and simplified representations of physico-chemical SOC protection [e.g., MIMICS, CORPSE, etc.] (Sulman et al., 2018; Wieder et al., 2015), even these newer models omit redox processes and interactions with micronutrients. These omissions limit the ability of SOC models to reproduce variations in SOC cycling across soils with different geochemical properties and parent materials (Doetterl et al., 2015; Kramer & Chadwick, 2018; Lehmann et al., 2020) and make it difficult for models to represent pH and redox effects.

Manganese (Mn) is a redox-active micronutrient that influences ecosystem C cycling by enabling photosynthesis (Broadley, Brown, Cakmak, Rengel, & Zhao, 2012), facilitating litter decomposition (Björn Berg et al., 2015; Davey, Berg, Emmett, & Rowland, 2007; Keiluweit et al., 2015; Sun et al., 2019), and (de)stabilizing organic compounds through organo-mineral interactions (Li, Santos, Butler, & Herndon, 2021; Remucal & Ginder-Vogel, 2014; Stone & Morgan, 1984). Dissolved Mn^{2+} in soil solution is moved through the roots and transported primarily to leaves where it accumulates as dissolved or organic-bound Mn^{2+} and is not remobilized to other plant tissues or reabsorbed during senescence (Fernando & Lynch, 2015; E. M. Herndon, C. E. Martínez, & S. L. Brantley, 2014; McCain & Markley, 1989). In soils where Mn is readily soluble as bioavailable Mn^{2+} or where changes in land cover favor Mn-accumulating plants, seasonal uptake and litterfall result in Mn accumulation in surface soils after mere decades (Jobbágy & Jackson, 2004; Oh & Richter, 2005). Microbial Mn oxidation facilitates Mn retention in surface soils by converting readily soluble foliar Mn^{2+} to insoluble Mn(III/IV) oxides (E. M. Herndon et al., 2014; Keiluweit et al., 2015).

High Mn^{2+} concentrations in leaf litter and organic horizons are proposed to reduce soil C storage by accelerating decomposition (Kranabetter, 2019; Santos & Herndon, 2023; Stendahl, Berg, & Lindahl, 2017). Soil fungi within Basidiomycetes produce extracellular Mn-dependent peroxidase (MnP) enzymes that convert Mn^{2+} to diffusible Mn^{3+}-chelates that indiscriminately oxidize phenolic bonds within lignin and polyphenols (Hofrichter, 2002; Keiluweit et al., 2015; Kellner et al., 2014; Morgenstern, Klopman, & Hibbett, 2008). This process degrades litter by generating organic radicals that depolymerize and destabilize lignin structures (Hatakka, Lundell,

Hofrichter, & Maijala, 2003). Other ligninolytic enzymes, e.g., lignin peroxidase (LiP) and laccase, are present at much lower activities in litter layers of boreal, temperate, and tropical forests (Fujii et al., 2020); thus, MnPs regulate litter decomposition rates and the extent to which litter decays by controlling lignin oxidation.

Positive correlations between decomposition rate and Mn concentrations in leaf litter have been observed across multiple tree species in forest-dominated ecosystems (Björn Berg et al., 2015; B. Berg, Steffen, & McClaugherty, 2006; Davey et al., 2007), presumably because MnP production and activity increase in response to high Mn^{2+} levels (Sun et al., 2019; Whalen, Smith, Grandy, & Frey, 2018). Furthermore, experimental additions of aqueous Mn^{2+} to forest soils stimulate soil respiration and CO_2 release (Li et al., 2021; Trum, Titeux, Cornelis, & Delvaux, 2011; Trum, Titeux, Ponette, & Berg, 2015). These effects may be attributed to Mn-promoted lignin decomposition that increases lignin and thus litter C loss over long timescales (Huang et al., 2023; Yi et al., 2023). However, the ecosystem-scale implications of these complex biogeochemical interactions remain to be explored.

Many existing models assume that litter decomposition rate is a fixed function of lignin content or lignin:nitrogen ratio and that SOM decomposition rate is influenced only by SOM quality and (in some models) microbial biomass (Parton, 1998; Sulman et al., 2018). Emerging model frameworks are beginning to include geochemical and redox interactions in wetland soils (Sulman et al., 2022). However, observed impacts of Mn concentrations on both litter decomposition and SOC turnover suggest that existing models may miss an important process by which both litter and SOC decomposition in upland soils respond to geochemical factors. For example, the ratio of Mn/lignin in litter is positively correlated with MnP activity and has been proposed as a cross-biome metric of degradability (Fujii et al., 2020). The role of vegetation in redistributing Mn through soil profiles (Herndon, Jin, Andrews, Eissenstat, & Brantley, 2015; Jobbágy & Jackson, 2004; Oh & Richter, 2005) further suggests that rates of lignin and SOC turnover could change over decadal time scales as a consequence of changing Mn solubility in response to soil acidification, moisture, or warming.

The objective of this study was to apply a model framework coupling Mn and C cycles to understand the role of these interactions in driving SOC and litter C stocks. First, we modeled interactions between plant-soil Mn cycling and soil C storage in a temperate forest (Figure 1). Plant uptake of Mn and accumulation in foliage was dependent on Mn^{2+} solubility in soil, a function of the dissolution of birnessite ($Mn^{III/IV}$-oxide), which depended on pH, soil redox status, and the precipitation/dissolution rate constant k_m (see Eq. 1) which we used to broadly represent the sensitivity of birnessite dissolution to inherent mineral properties (e.g., crystallinity) and to undefined environmental factors. A Mn-dependent decomposition pathway was introduced by using Mn concentrations in leaf litter to regulate the rate that lignin was oxidized to produce labile dissolved organic matter (DOM). Subsequent DOM respiration and leaching influenced C redistribution and net storage in organic and mineral horizons. We also tested the interaction of soil hydrology with Mn redistribution and leaching losses by simulating periodic and depth-dependent soil saturation representing a gradient from well to poorly drained soils. Second, we

explored how Mn cycling and coupled soil C storage respond to soil warming that is consistent with ongoing climate change. Finally, we examined how interactions between Mn and N addition influenced C storage under different warming scenarios through simulated N-inhibition of Mn-dependent oxidative enzymes (Moore et al., 2020; Whalen et al., 2018).

2 Materials and Methods

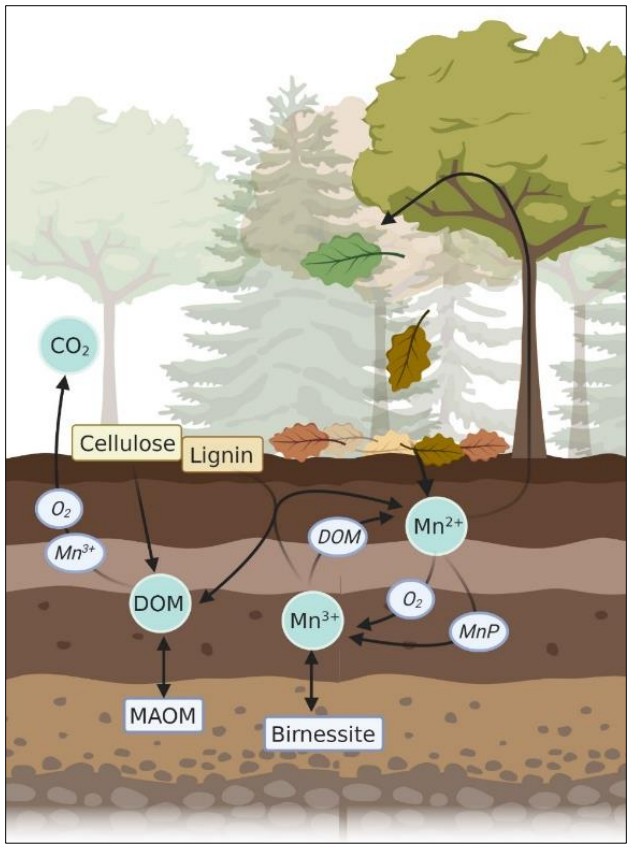

Figure 1. Conceptual model representing the simplified manganese (Mn) – carbon (C) cycling reaction network in a forest ecosystem. Arrows indicate the transformation of one species to another as mediated by reaction with other system components, represented by either intersecting arrows or as white circles over the arrow. Solid-phase species are shown as rectangles while aqueous and gaseous species are shown as blue circles. Abbreviations indicate dissolved organic matter (*DOM*), mineral-associated organic matter (*MAOM*), and Mn peroxidase (*MnP*). Reactions are not balanced. Image created with *BioRender.com.*

2.1. Model description

The model configuration represents a soil profile in a temperate forest consisting of a surface forest floor layer comprised of leaf litter and an organic horizon (0 – 5 cm with a bulk density of 0.5 g cm^{-3}) and four underlying mineral horizons (each 10 cm thick with a bulk density of 1.5 g cm^{-3}), for a total profile depth of 45 cm including the forest floor layer. At time zero, the forest floor layer contains no Mn while the mineral horizons contain a uniform distribution of Mn (28 mmol kg^{-1}) hosted in the mineral birnessite ($Mn^{III,IV}O_2$; average oxidation state = 3.7) and 0.3 mmol kg^{-1} exchangeable Mn^{2+}. Soil properties, including total and exchangeable Mn concentrations, are based on values reported for the Susquehanna Shale Hills Critical Zone Observatory (SSHCZO), a temperate forested watershed in central Pennsylvania, U.S.A where Mn cycling through vegetation has been documented (Brantley et al., 2018; E. Herndon, C. E. Martínez, & S. Brantley, 2014; Herndon et al., 2015; Jin et al., 2010). Our initial soil Mn

concentration is intermediate between depth-averaged Mn concentrations in ridgetop mineral soils at this site (41 ± 4 mmol kg^{-1}; n = 120) and average Mn concentrations in A horizons of upland deciduous forests of the conterminous United States (16 ± 15 mmol kg^{-1}; n = 777) (D. B. Smith et al., 2013). Soil Mn at SSHCZO is dominated by Mn oxides such as birnessite (E. Herndon et al., 2014). Other solid phase Mn that may be present in the soil, such as Mn present in silicate minerals, is considered non-reactive over the time frame of the model.

The model was implemented in the reactive transport model PFLOTRAN (Hammond, Lichtner, & Mills, 2014) using a python driver via the Alquimia interface (Andre, Molins, Johnson, & Steefel, 2013). A simplified summary of the reaction network used in our simulations is shown in Figure 1, and reaction equations are provided in Table 1. Reactions in the model are assumed to occur in aqueous phase, except for cellulose and lignin depolymerization. Mn ions involved in reactions include divalent (Mn^{2+}) and trivalent (Mn^{3+}) species, with Mn^{3+} existing in either a meta-stable chelated state (formed in solution following Mn^{3+} production by the MnP enzyme) or quasi-instantaneously precipitating to birnessite. We consider only diffuseable Mn^{3+} bound to small organic molecules and do not include Mn^{3+} ions that complex with solid-phase organic matter (e.g., pyrophosphate-extractable Mn; (Jones et al., 2020; Possinger et al., 2022). The availability of Mn^{3+} for aqueous reactions is calculated using transition state theory rate laws implemented in PFLOTRAN (Dwivedi, Arora, Steefel, Dafflon, & Versteeg, 2018) (Dwivedi et al., 2018; Lichtner et al., 2020 (Lichtner et al., 2015)) for kinetic precipitation/dissolution of birnessite, which is highly sensitive to pH due to the stoichiometry of the reaction:

$$I_m = -k_m\left(1 - \left(K_m[\mathrm{H}^+]^{-21}[\mathrm{Mn}^{3+}]^7\right)^{1/7}\right) \quad (1)$$

where I_m is the precipitation/dissolution rate (mol m^{-3} s^{-1}); k_m is the reaction rate constant (mol m^{-3} soil s^{-1}); and K_m is the equilibrium constant ($10^{-5.5}$). The actual Mn^{3+} concentration is very low (on the order of 10^{-15} mol L^{-1}) due to its high reactivity, but Mn^{3+} concentration does respond to removal via Mn^{3+} reduction or production via Mn^{2+} oxidation, connecting the precipitation/dissolution of birnessite to the associated Mn redox processes. We simulated a range of birnessite precipitation/dissolution rate constants (k_m) from 2.5×10^{-13} to 6.4×10^{-11} mol m^{-3} s^{-1} to represent a gradient of mineral properties (e.g., crystallinity, surface area) and other environmental factors (e.g., microbial biomass) that potentially influence dissolution rates (Bandstra et al., 2011). The sign of Eq. 1 (indicating the direction of precipitation versus dissolution) and the actual reaction rate are sensitive to the ratio of proton concentration to Mn^{3+} concentration, making the actual precipitation/dissolution rate and direction sensitive to pH and Mn^{3+} concentration as well as the factors implicitly included in the rate constant.

Monod type reactions in the model can include multiple Monod and inhibition factors:

$$R = V_{max} \prod_N \frac{C_{S_N}}{K_{S_N} + C_{S_N}} \prod_M \frac{K_{I_M}}{K_{I_M} + C_{I_M}} \quad (2)$$

where R is reaction rate (M s^{-1}), V_{max} is maximum reaction rate (M s^{-1}), N is the set of reactant species (including substrate and terminal electron acceptors), M is the set of inhibiting species, C_{S_N} is the concentration of the Nth substrate, K_{S_N} is the half-saturation constant of the Nth substrate, C_{I_M} is the concentration of the Mth inhibiting species, and K_{I_M} is the inhibition constant of the Mth inhibiting species.

Litter and soil organic matter in the model are represented as cellulose and lignin that are degraded to form dissolved organic matter (DOM). Lignin, cellulose, and DOM are tracked on a per unit C basis (Table 1). The combination of cellulose and lignin pools are interpreted as total particulate organic matter (POM). Cellulose is depolymerized to DOM at a constant first-order rate that is independent of Mn concentration. Depolymerization of lignin to DOM occurs via a Mn peroxidase (MnP) enzymatic reaction. MnP in the model converts Mn^{2+} to Mn^{3+}, which is chelated and then reacts directly with lignin to produce decomposable DOM. The rate of chelated Mn^{3+} production, and thus the rate of MnP-mediated lignin depolymerization, increases with Mn^{2+} concentration, representing the catalytic use of Mn^{2+} by MnP and increased fungal MnP production with increasing Mn^{2+} (Björn Berg et al., 2015; Davey et al., 2007; Sun et al., 2019; Whalen et al., 2018). The model also includes a slower Mn-independent lignin depolymerization pathway representing alternative enzymatic pathways for lignin degradation, assumed to be about an order of magnitude slower than Mn-dependent lignin degradation. In addition to reacting with lignin, chelated Mn^{3+} can also decompose spontaneously via disproportionation to Mn^{2+} and oxidized Mn^{4+} which immediately precipitates to birnessite, as has been proposed to occur upon cessation of microbial Mn recycling (Keiluweit et al., 2015). Bacterial oxidation of Mn^{2+} by O_2 is also included as a separate reaction (Tebo et al., 2004).

DOM oxidation by O_2 to CO_2 occurs under oxic conditions. DOM can also be oxidized to CO_2 via microbial Mn^{3+} reduction (occurring only under anoxic conditions) (Bandstra, Ross, Brantley, & Burgos, 2011) or via abiotic Mn^{3+} reduction which can occur under anoxic or oxic conditions. Because Mn^{3+} reduction consumes reactive Mn^{3+} ions that are near equilibrium with birnessite, these Mn reduction reactions drive reductive dissolution of birnessite in the model. The rate of birnessite dissolution increases with decreasing pH (which increases birnessite solubility and Mn^{3+} ion availability), higher DOM concentration (which accelerates the rate of Mn^{3+} consumption via the Mn reduction reaction, allowing additional birnessite dissolution to maintain equilibrium), and lower oxygen concentration (because the Mn reduction reaction rate is inhibited by oxygen).

DOM can also be stabilized via sorption to mineral surfaces in mineral horizon layers to become mineral-associated organic matter (MAOM). MAOM formation and desorption are represented as saturating and first-order transformations, respectively, rather than explicitly simulating mineral surface sorption interactions. Solutes in the model are transported downward over time at a fixed flow rate (10^{-7} cm s^{-1}). Layers under oxic conditions are assumed to be at equilibrium with the atmosphere for both O_2 (20%) and CO_2 (400 ppm). Because gas transport is assumed to be much slower under saturated conditions, low O_2 availability limits organic matter decomposition under saturated conditions typical of more poorly drained soils.

Root uptake of Mn^{2+} occurs in each layer at a rate proportional to the root biomass profile, which decreases exponentially with depth in the mineral layers (Fig. S6). Plant uptake of Mn is strongly dependent on its concentration in soil solution (Kabata-Pendias & Pendias, 2001). The forest floor layer, which represents the organic horizon and fresh leaf litter inputs, is assumed to have low root biomass. Note that this approach may lead to underestimates of root Mn uptake from organic layers which can have high concentrations of root biomass in the field. However, because

the forest floor layer was assumed to be oxic and soluble Mn could be leached downward, this assumption did not substantially affect total root Mn uptake. Focusing on root Mn uptake from deeper layers did allow the study to focus on vertical redistribution of Mn. Roots are assumed to maintain charge balance by exuding protons in proportion to Mn^{2+} uptake (Haynes, 1990). At the end of each simulated year, all Mn^{2+} taken up by roots over the year is deposited to the forest floor along with a constant mass (0.163 kg C m^{-2} $year^{-1}$) of litter C reported for a temperate forest (L. A. Smith, Eissenstat, & Kaye, 2017). Thus, leaf litter Mn^{2+} concentrations change over time in response to total root Mn^{2+} uptake.

The impact of N deposition on decomposition was modeled by including an inhibiting effect of NH_4^+ concentration on the MnP reaction (Eq. 1) with a half-saturation constant of 0.01 M. Although our model uses direct inhibition to simulate the observed suppression of ligninolytic enzyme activity by N enrichment, previous studies have proposed indirect mechanisms such as changes to microbial community structure and function (Entwistle, Romanowicz, Argiroff, & Zak, 2019; Whalen et al., 2018). Different rates of N deposition were represented by adding NH_4^+ to the forest floor at a constant rate during each simulation. N deposition rates of 0 (no N deposition), 50, and 150 kg N ha^{-1} y^{-1} were simulated, based on the amounts applied by (Whalen et al., 2018). Warming levels up to +5 ºC were simulated by altering the rates of all microbial (Monod-type and organic matter decomposition) reactions in the reaction network assuming a temperature dependence with a Q_{10} of 2.0 (meaning a doubling of reaction rates with every 10ºC increase in temperature). Affected reactions included lignin oxidation by MnP, Mn^{3+} reduction to Mn^{2+} (which drove reductive dissolution of birnessite during anoxia), Mn^{2+} oxidation to Mn^{3+} by O_2, cellulose decomposition, and DOM oxidation. Thus, rates of Mn-oxide dissolution and precipitation, Mn^{2+} oxidation by MnP, and C cycling were accelerated in warming scenarios. All N deposition and warming simulations were conducted at initial soil pH levels of 4.0, 4.5, 5.0, 5.5, and 6.0 given that Mn solubilization and redistribution were negligible above pH 6.

2.2. Model parameterization

The primary model parameters were rate constants and half-saturation constants for the Monod-type reactions that formed the basis of the biogeochemical reaction network (Table 1). The model was also sensitive to relative rates at which chelated Mn^{3+} either reacted with lignin or underwent disproportionation and precipitated to birnessite. Where available, existing measurements were used to inform model parameter values. However, direct observational constraints on parameter values were highly limited due to the lack of direct observations of MnP and other enzymatic rates across gradients of substrate availability. While some laboratory measurements were available from previous studies involving microbial Mn oxidation and reduction reactions, these measurements were generally conducted under highly controlled laboratory conditions (Bandstra et al., 2011; Tebo et al., 2004) that were not immediately comparable to field soil conditions. Thus, our approach for model parameterization primarily relied on using inverse modeling to select a combination of parameter values that yielded simulation results consistent with observed patterns of leaf Mn concentration (B. Berg et al., 2013;

E. M. Herndon et al., 2014), soil Mn concentrations (E. M. Herndon et al., 2014; Jin et al., 2010), and leaf mass loss over time (B. Berg et al., 2013; Davey et al., 2007). We conducted simulations across a range of values for key parameters including rate constants and half-saturation constants of lignin depolymerization, chelated Mn^{2+} disproportionation, and Mn reduction and oxidation (Table 1), and selected the combination of parameters that qualitatively matched the observed ranges of both leaf Mn concentrations and leaf mass loss (Fig. S2) as well as reasonable values of soil Mn concentration profiles in the context of the aforementioned references. This parameterization procedure was somewhat qualitative due to the multiple data types (listed above) that we used as a basis of comparison. A rigorous statistical comparison between measured and modeled data points was not possible because the model predicted both leaf Mn concentration and leaf mass loss based on a combination of environmental factors. As a result, there was not a one-to-one relationship between modeled and measured points in Fig. S2.

2.3. Model simulations

We conducted multiple simulations with a length of 80 years and a time step of six hours, testing different combinations of initial soil pH, birnessite precipitation/dissolution rate constants, warming levels, and N deposition rates. This set included 5 pH × 5 precipitation/dissolution rate constants × 3 N deposition rates × 3 warming levels, for a total of 225 simulations. We also conducted four additional simulations with different drainage time scales to represent a gradient of poorly to well-drained hydrological settings, using pH = 5.0 and the middle birnessite dissolution rate constant. Hydrology was simulated by assuming 50 precipitation events occurred per year (evenly distributed in time). Following each precipitation event, each soil layer was assumed to be saturated (limiting oxygen diffusion into the layer) for a length of time determined by the drainage time scale (ranging from 0.25 to 2 days) and depth:

$$t_{anox} = t_{drain} e^{\frac{z}{0.125}} \quad (3)$$

Where t_{anox} is the length of time the layer remains saturated, t_{drain} is the drainage time scale, and z is the depth of the middle of the layer. Figure S1 shows how these drainage time scales translated into the fraction of time that each layer was saturated as a function of depth and drainage time scale.

2.4. Factors not addressed in the current model

While our modeling approach incorporates key biogeochemical factors relevant to Mn-C interactions in soils, it does omit some important processes that should be considered when interpreting the results. First, the model uses a simple approach to the vegetation component, assuming that root uptake of Mn is controlled only by a static rooting depth distribution and that Mn taken up during the year is directly deposited into the forest floor with litterfall (Herndon et al., 2015). The model does not consider the effect of Mn availability on photosynthetic processes (Gonzalez & Lynch, 1997; St. Clair & Lynch, 2004), variations in leaf Mn content among tree species (Herndon et al., 2015; Kogelmann & Sharpe, 2006; St. Clair & Lynch, 2005) or sun versus shade leaves (McCain & Markley, 1989), or variations in leaf lignin content. Variations in

335 microbial communities or microbial physiology over space or time were also not included due to
336 lack of data available to constrain community composition and key microbial parameters such as
337 growth and mortality rates with respect to Mn-related microbial community function. Fixed model
338 parameters, such as the rate constant for Mn^{2+} oxidation by MnP and other microbial-mediated
339 reactions, or the partitioning of C between CO_2 and DOM, could in fact vary over time through
340 microbial community or physiological changes. The representation of soil organic matter was quite
341 simple, including only cellulose, lignin, DOM, and MAOM that formed and desorbed at fixed
342 rates. Variations in DOM composition and a more complex representation of POM could lead to
343 different results. Our model included a somewhat simple approach to litter decomposition focused
344 on MnP as well as a single Mn-independent lignin depolymerization process. However, other
345 biological processes including faunal decomposers such as earthworms could also act as a limit on
346 litter accumulation under low-Mn conditions, and abiotic processes such as fire or photooxidation
347 could facilitate lignin decomposition.
348

349 ## 3 Results and Discussion

350 ### *3.1. Enhanced biological Mn cycling decreases C storage*

351 Mn bioavailability and forest floor Mn stocks depended strongly on soil pH and birnessite k_m
352 and were highest in acidic soils where enhanced birnessite dissolution increased Mn availability
353 for root uptake (Figure 2, S3). Leaf litter Mn concentration and forest floor bioavailable Mn were
354 in turn strongly correlated with Mn bioavailability in the soil column (Figure 3). POM C stocks
355 (kg C m^{-2}) were inversely related to litter Mn concentrations and soil Mn bioavailability (Figure
356 3a), reflecting the role of Mn^{2+} concentration in MnP-mediated lignin depolymerization.
357 Specifically, faster and more complete lignin decomposition reduced POM C stocks from 1.55 kg
358 C m^{-2} where Mn bioavailability was low to 1.2 kg C m^{-2} where Mn bioavailability was high, a 23%
359 reduction over 40 years (Figure 2a). The simulated ranges of leaf Mn concentrations and one-year
360 lignin mass loss, as well as the positive relationship between leaf Mn concentration and lignin
361 mass loss, were consistent with observations of one-year lignin decomposition across a range of
362 leaf litter Mn concentrations (Björn Berg et al., 2015) (Figure S2), although the model did not
363 reproduce the higher end of leaf Mn concentrations.
364

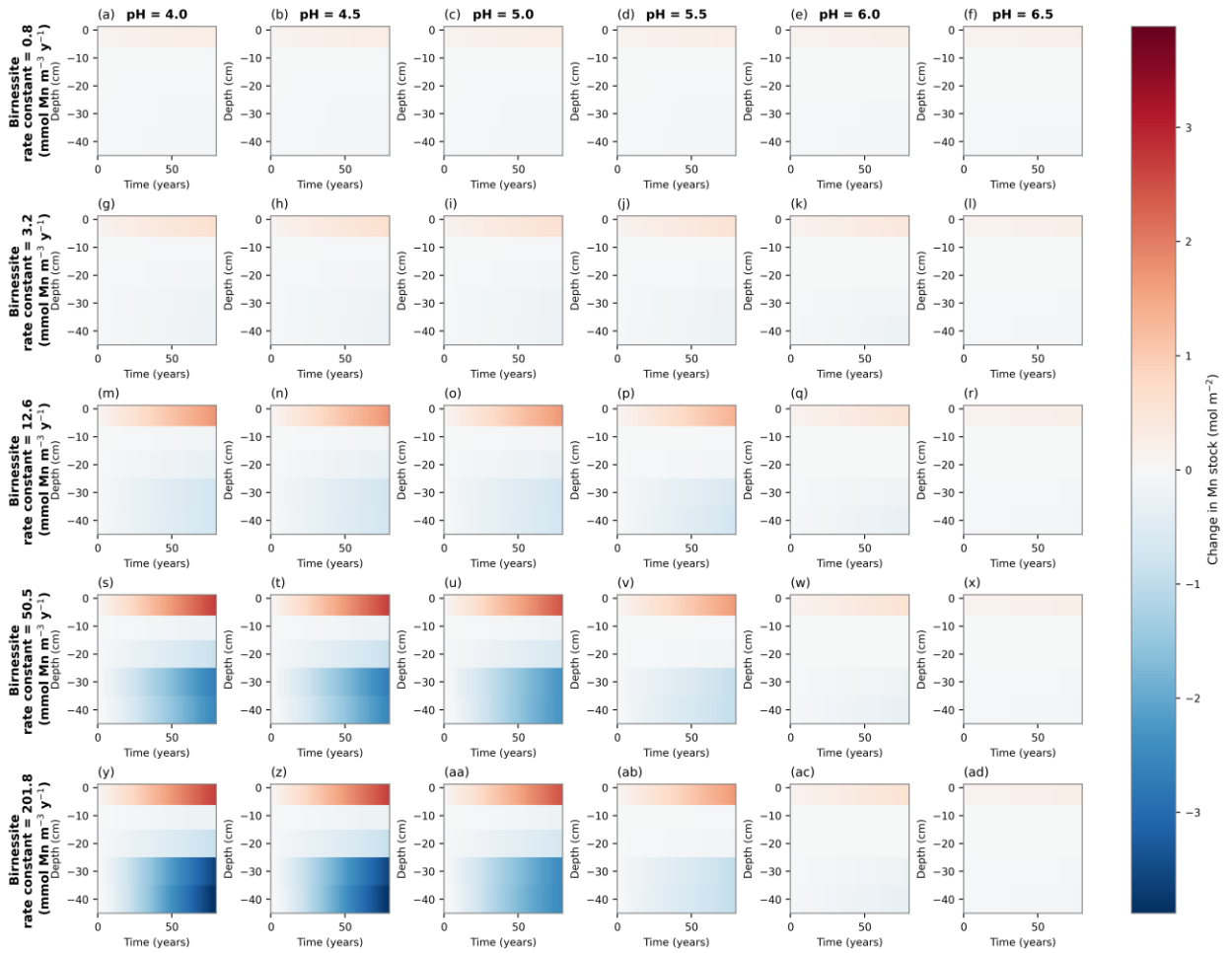

Figure 2. Mn redistribution in the soil profile: Redistribution of Mn across soil layers as a function of time for five initial soil pH levels from 4.0 to 6.5 and five rate constants of birnessite dissolution. Soil layers include the forest floor (0 – 5 cm) and four mineral layers (each 10 cm thick). The color gradient indicates increases (red colors) or decreases (blue colors) in Mn stock (mol m^{-2}) in each layer relative to initial stocks. More pronounced Mn redistribution from deep soil layers to the surface organic layer occurs at lower pH and higher birnessite dissolution rate constant.

Mn-promoted depolymerization of lignin in the forest floor increased fluxes of DOM to underlying mineral soil layers, but this effect was counteracted by increased Mn^{3+} reduction which served as a sink for DOM. These combined effects drove an increase in total MAOM from very low to moderate levels of bioavailable Mn, but a decrease in MAOM at the highest levels of Mn bioavailability as more C was released as CO_2 (Figure 3d). Neupane et al. (2023) similarly reported increased CO_2 production and C transfer from POM to MAOM stocks with Mn addition to agricultural soils (Neupane, Herndon, Whitman, Faiia, & Jagadamma, 2023). Overall, total soil C stocks, including the forest floor and mineral soil layers, decreased with higher bioavailable Mn (Figure 4c), similar to patterns observed across multiple biomes (Kranabetter, 2019; Santos & Herndon, 2023; Stendahl et al., 2017).

383 Modeled litter Mn concentrations were comparable to measured foliar Mn (~6 to 60 mmol kg^{-1}) in forests growing on acidic soils (pH 3.4 to 5.3) in the northeastern United States, where higher concentrations are observed for deciduous trees and at lower pH (Herndon et al., 2015; Kogelmann & Sharpe, 2006; Richardson, 2017; St. Clair & Lynch, 2005) (Figure S2). Simulated concentrations were higher than concentrations reported in the literature only for soils with both very low pH (< 4.5) and high rates of birnessite dissolution.

389 Total soil Mn was redistributed upward within the soil profile over time in our model due to plant uptake of Mn^{2+} from the subsurface and redeposition in litter on the soil surface (Figure 2), consistent with field observations (Herndon et al., 2015; Jobbágy & Jackson, 2004). Redistribution was most pronounced at low pH and more rapid mineral dissolution rates. Over 80 years, strongly acidic soils (pH ≤ 5) accumulated up to 3 mol m^{-2} total Mn in the forest floor layer, while moderately acidic soils (pH > 5) accumulated < 1 mol m^{-2}. Deep mineral horizons showed comparable Mn depletion. Mn that accumulated in the forest floor persisted as bioavailable exchangeable Mn^{2+} at low pH but was mostly converted to birnessite at higher pH (Figure S3). Poorly drained soils had higher vertical Mn redistribution than well-drained soils due to the enhancement of reductive dissolution of birnessite in subsurface soil layers that were exposed to longer periods of saturated conditions (Figure S4). Poorly drained soils and soils with higher birnessite dissolution k_m also had higher rates of Mn leaching out of the system (Figure S5). The rate of leaching was not enough to substantially deplete Mn stocks over the multidecadal time scale of our simulations but could contribute to Mn limitation over longer time scales. Redistribution of Mn^{2+} towards the soil surface may further facilitate Mn-promoted decomposition in surface soils (Jones et al., 2020).

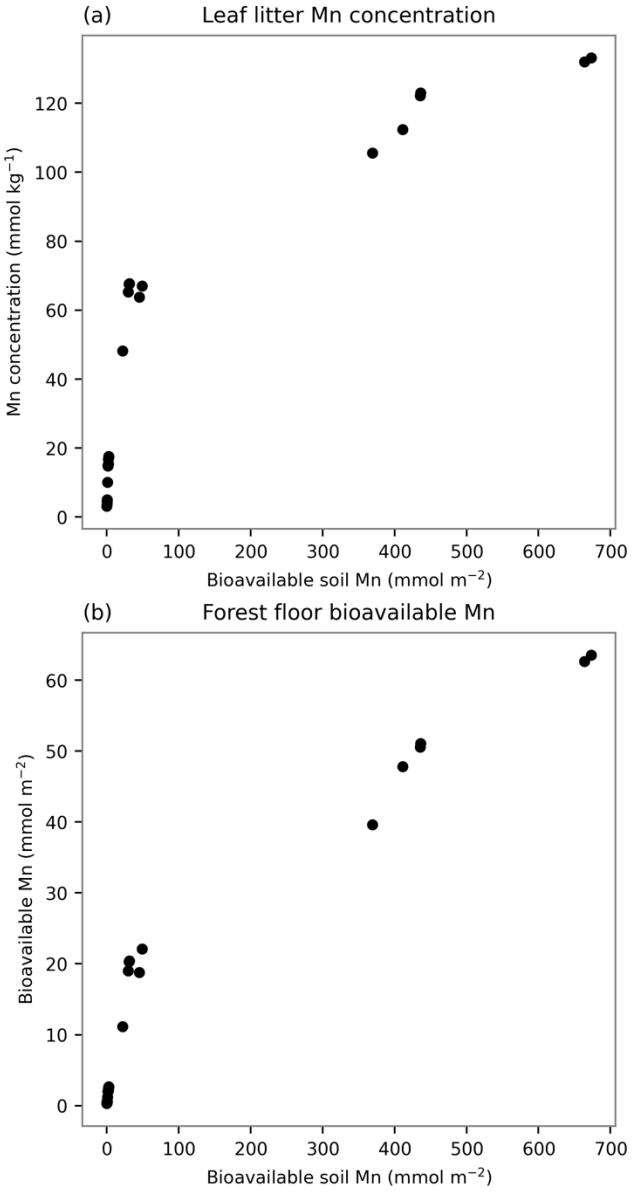

Figure 3. High Mn in leaf litter and surface soils with increasing Mn solubility in the soil profile. Mn concentrations in leaf litter (a) and Mn bioavailability in the forest floor and (b) as a function of bioavailable soil Mn integrated across the entire soil profile.

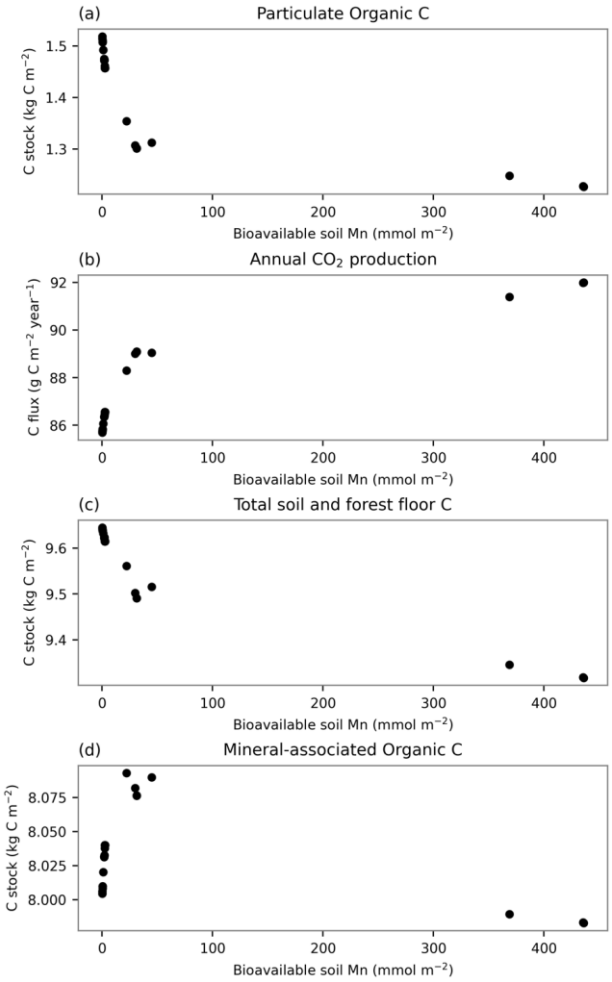

Figure 4. High Mn bioavailability leads to less C accumulation in litter and soils. (a) POM C stocks (kg C m^{-2}) integrated across forest floor (5 cm) and mineral soil (40 cm) layers, (b) annual CO_2 production, and (c) total organic C (kg C m^{-2}) stocks contained in both forest floor and mineral soil across a range of bioavailable soil Mn that varies with soil pH and birnessite dissolution rate.

3.2. Mn availability modulates effects of soil warming on decomposition

Soil warming is expected to decrease soil C stocks by increasing rates of microbial decomposition of organic matter, but warming responses can be complicated by biological, chemical, and physical factors controlling organic matter chemistry and availability (Conant et al., 2011). Increasing temperatures have the added effect of accelerating mineral dissolution and precipitation reactions. Our model simulated warming by increasing the reaction rates of all microbially-mediated reactions using a Q_{10} temperature sensitivity function.

Warming reduced POM C stocks due to higher decomposition rates, but the strength of the warming effect was moderated by Mn bioavailability (Figure 5). At higher levels of underlying Mn bioavailability (faster birnessite k_m), warming increased soil bioavailable Mn and leaf litter Mn concentration (Figure 5a,c). However, at lower levels of underlying Mn bioavailability, warming decreased soil bioavailable Mn and leaf litter Mn concentrations. This led to differential effects of warming on soil carbon loss depending on soil Mn availability. The warming response was strongest at higher levels of soil Mn availability, as warming further enhanced Mn availability and drove faster decomposition (Figure 5e). By contrast, the warming impact on C stocks was weaker at lower levels of Mn availability, with Mn limitation of MnP-mediated lignin decomposition leading to less overall C loss. This suggests that warming effects on litter decomposition could be sensitive to soil Mn availability.

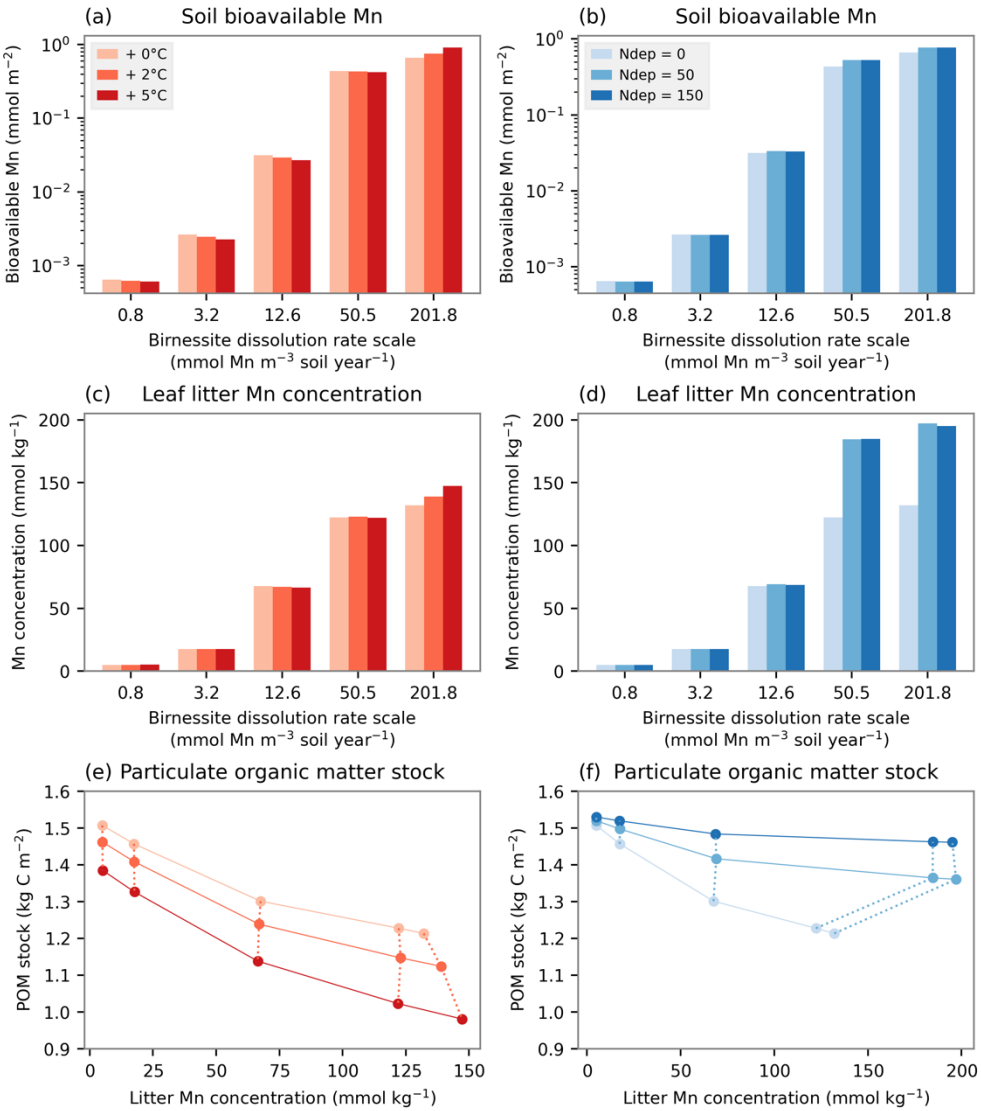

Figure 5. N deposition and warming effects on coupled C-Mn cycling. Simulations with initial soil pH of 4.5 are shown across a range of birnessite k_m. All values are after 40 years of simulated time. (a): Soil bioavailable Mn stock as a function of birnessite dissolution $k_m$and warming treatment. (b): Soil bioavailable Mn as a function of birnessite dissolution $k_m$and N deposition treatment. (c,d): Leaf litter Mn as a function of birnessite dissolution k_m and warming or N deposition. (e,f): Soil POM C stocks as a function of litter Mn concentration and warming or N deposition. Solid lines connect simulations with the same warming or N deposition treatment, and dashed lines connect simulations with the same birnessite dissolution k_m.

3.3. N enrichment limits Mn-dependent lignin decomposition

Chronic N deposition to soils can increase litter C stocks by downregulating ligninolytic enzyme production (Chen et al., 2018; Entwistle et al., 2019; Frey et al., 2014; Zak et al., 2019). Although most studies do not differentiate between specific ligninolytic enzymes, MnP has been implicated as the most ubiquitous and important enzyme involved in this process (Entwistle et al.,

2019). We tested interactive effects of Mn and N on lignin degradation and consequent C storage in the forest floor. Soil Mn bioavailability interacted with different levels of N deposition to control lignin degradation rates (Figure 5b,d,f). Higher rates of N deposition suppressed MnP activity, as simulated based on previous observations (Moore et al., 2020; Whalen et al., 2018). As a result, N deposition increased C stocks and weakened the dependence of C stocks on Mn bioavailability (Figure 5f).

Thus, model results indicate that the negative impact of N addition on MnP activity could limit degradation of lignin compounds and result in C accumulation. Paradoxically, N additions have also been shown to acidify soils and increase Mn uptake (Hou et al., 2021; Tian et al., 2016). Although the acidifying effect of N additions was not included in our model simulations, simulated N deposition did increase soil bioavailable Mn (Figure 5b) and leaf litter Mn concentrations (Figure 5d), most likely because N inhibited MnP-driven Mn oxidation in surface soil layers. Although not included in our model, excess Mn uptake in response to N addition can impair rates of photosynthesis and decrease biomass in sensitive species, ultimately shifting the quantity and composition of litter C inputs to soils (Tian et al., 2016). These counteractive effects may be limited to certain systems, as soils experiencing high levels of N addition do not necessarily experience concurrent decreases in soil pH (Zak et al., 2019). However, these complex Mn-N-C interactions are important to decipher given widespread N deposition derived from combustion and fertilization (Hou et al., 2021; Tian et al., 2016; Zak et al., 2019).

4 Conclusions

Our simulations demonstrate that interactions between C cycling and micronutrients, which are not included in ecosystem-scale C cycle models, may have an underappreciated but critically important role in regulating C storage and partitioning, particularly by regulating microbial decomposition of organic matter. Lignin oxidation is a rate-limiting step in decomposition models, which parameterize litter decomposition using lignin content (Parton, 1998; Zaehle et al., 2014). Because litter decomposition rates control both the buildup of organic C stocks in the forest floor and the transfer of DOM into underlying mineral soil via leaching, the high sensitivity of lignin oxidation to Mn availability represents an important control on both surface and subsurface soil C cycling that is omitted in most models. Our simulations suggest that such models may underestimate the variability of litter decomposition rates across sites with different Mn availabilities, with important consequences for model simulations of soil C stocks. The key role of Mn availability in lignin oxidation suggests that efforts to increase ecosystem C sequestration by selectively cultivating or engineering high lignin plant tissues (Garten, Wullschleger, & Classen, 2011; Hancock et al., 2007; Post et al., 2004) may need to take local geochemical factors into account as the efficiency of C sequestration in lignin-rich biomaterials could depend on soil Mn availability.

In addition, we find that previously documented interactions between N deposition and MnP activity (Whalen et al., 2018) could have consequences for ecosystem-scale C cycling that models

lacking these biogeochemical interactions will not be able to reproduce. Legacy N accumulation and ongoing deposition could increase C stocks by hindering lignin oxidation, while mitigation of atmospheric N deposition could have the opposite effect. Counteracting effects of Mn and N could create heterogeneous responses of litter decomposition to individual factors across ecosystems with different N and Mn availabilities, raising the difficulty of predicting litter decomposition rates across geographical areas.

Our simulations also suggest that Mn availability could moderate the response of organic C stocks to warming via feedback to Mn uptake that depends on soil Mn bioavailability. Conventional C cycle models assume that decomposition rates are determined by organic matter properties and climatic factors rather than geochemical factors, and thus would overestimate the increase in decomposition rates and consequent decline in soil C stocks in systems with low Mn availability. Warming studies have previously documented reduction in the impact of warming on soil respiration over time (Melillo et al., 2017; Romero-Olivares, Allison, & Treseder, 2017) which has been attributed to microbial physiological or community adaptation (Bradford, Watts, & Davies, 2010; Luo et al., 2014) or to depletion of labile C (Hartley, Heinemeyer, & Ineson, 2007; Kirschbaum, 2004). Our simulations suggest that depletion of Mn or other geochemical cofactors critical to decomposition could also explain reduction in warming responses over time and should be considered when interpreting warming impacts on decomposition and when simulating soil C responses to warming temperatures.

Although our model demonstrates the high sensitivity of C cycling to Mn cycling over decadal time scales, key model parameters, e.g., rates of Mn^{2+} oxidation by MnP in environmental systems, have not been well constrained. Furthermore, stimulatory effects of Mn on litter decomposition may be absent or difficult to identify across ecosystems owing to factors other than redox and pH that limit Mn bioavailability and/or influence litter decomposition (Kranabetter, Philpott, & Dunn, 2021; Li et al., 2021; Trum et al., 2011). For example, Mn accelerates transformation of litter and POM C but may not ultimately affect C storage because decomposed C is then retained in more stable pools (Possinger et al., 2022), possibly explaining negative correlations between soil Mn and soil C decomposition (Huang et al., 2023). In addition, soils that are highly weathered may contain crystalline Mn oxides that are poorly soluble, as simulated in this study by varying birnessite dissolution rates, or may become Mn depleted due to leaching of Mn from the soil over time (Kranabetter et al., 2021). Also, lignin peroxidase rather than MnP may dominate decomposition in organic soil layers that underlie litter (Fujii et al., 2020; Fujii, Uemura, Hayakawa, Funakawa, & Kosaki, 2013). Thus, the stimulatory effects of Mn on decomposition may not always translate to decreases in soil C storage. Measurements and experiments to improve constraints on ecosystem Mn cycling across gradients of climate and soil types could yield important insights for C cycle responses to climate change. This model structure can be used to couple micronutrient cycling with C and N dynamics to explore complex ecosystem response to warming climate.

Acknowledgments

This work was sponsored by the Laboratory Directed Research and Development Program of Oak Ridge National Laboratory, managed by UT-Battelle, LCC for the US Department of Energy under contract DE-AC05-00OR22725, and was in part supported by a grant from the National Science Foundation Geobiology and Low-temperature Geochemistry program (EAR–1749849). This research used resources of the Compute and Data Environment for Science (CADES) at the Oak Ridge National Laboratory, which is supported by the Office of Science of the U.S. Department of Energy under Contract No. DE-AC05-00OR22725. The Alquimia biogeochemistry API and wrapper library was originally developed as part of the DOE ASCEM project and is an interoperable component of the Department of Energy's IDEAS-Watersheds (https://ideas-productivity.org/) software productivity project. BNS and EMH were also supported by the U.S. Department of Energy Office of Science Early Career Research program as part of research in Earth System Model Development within the Earth and Environmental Systems Modeling Program (BNS) and through Environmental Systems Science (EMH) within the Biological and Environmental Research program.

Open Research

Full model output will be made publicly available with an attached DOI through the ORNL Constellation repository (https://doi.ccs.ornl.gov/). Model output and code are currently posted at https://www.dropbox.com/scl/fi/ijbd0vt5c5l4k77bchu1o/Mn_output_2024-03-03_00.nc?rlkey=d4ozm516z6l6c6nqgqfrd2o4l&dl=0.

Table 1. Reactions and rate constants included within the model reaction network. Multiple rate constants are shown for Birnessite precipitation-dissolution because multiple values were used in different simulations.

Reaction	**Stoichiometry**	**Rate law**	**Rate constant**
Cellulose depolymerization	$\mathrm{Cellulose} \rightarrow \mathrm{DOM}$	First order rate	0.004 d^{-1}
Lignin depolymerization	Lignin → DOM	First order rate	0.00034 d^{-1}
Mn^{2+} oxidation by MnP	$Mn^{2+} + H^+ \rightarrow Mn^{3+}$(chelate)	Monod dependence on Mn^{2+} (k=0.1 mM)	1.7×10^{-4} mol L^{-1} d^{-1}
Mn-dependent lignin depolymerization	$\mathrm{Lignin} + Mn^{3+}(\mathrm{chelate}) \rightarrow \mathrm{DOM} + Mn^{2+} + H^+$	First order rate	0.002 d^{-1}
Chelated Mn^{3+} disproportionation	2 Mn^{3+}(chelate) + 0.5 H_2O → Mn^{2+} + Mn^{3+} + 0.25 O_2 + H^+	First order rate	0.01 d^{-1}
Bacterial Mn^{2+} oxidation	$Mn^{2+} + H^+ + 0.25\ O_2 \rightarrow Mn^{3+} + 0.5\ H_2O$	Monod dependence on O_2 (k=0.1 mM)	8.6×10^{-7} mol L^{-1} d^{-1}
Microbial Mn reduction	$\mathrm{DOM} + 4\ Mn^{3+} \rightarrow CO_2 + 4\ Mn^{2+} + 4\ H^+$	Monod reaction, inhibited by O_2	4.3×10^{-6} mol L^{-1} d^{-1}
Aerobic DOM oxidation	$\mathrm{DOM} + O_2 \rightarrow CO_2$	Monod dependence on O_2 (k=0.1 mM)	8.6×10^{-3} mol L^{-1} d^{-1}
Abiotic Mn reduction	$\mathrm{DOM} + 4\ Mn^{3+} + 2\ H_2O \rightarrow CO_2 + 4\ Mn^{2+} + 4\ H^+$	Aqueous complexing reaction, can happen under oxic conditions	8.6×10^{34} (mol L^{-1})$^{-4}$
Birnessite precipitation-dissolution	$7\ Mn^{3+} + 1.25\ O_2 + 15.5\ H_2O \leftrightarrow (Mn^{3+})_2(Mn^{4+})_5O_{13} * 5\ H_2O + 21\ H^+$	PFLOTRAN uses transition state theory[1]	(2.16, 8.64, 34.6, 138, 553) $\times10^{-6}$ mol Mn m^{-3} soil d^{-1}
DOM sorption	$\mathrm{DOM} \leftrightarrow \mathrm{DOM_S}$	$\frac{d}{dt}(\mathrm{DOM_S}) = k_1 * S_{max}\frac{\mathrm{DOM}}{k_S + \mathrm{DOM}} - k_2(\mathrm{DOM_S})$ k_S = 1 M S_{max} = 0.83 mmol C cm^{-3} (mineral layers)	k_1: 8.6×10^{-6} mol L^{-1} d^{-1} (S_{max} [mol C cm^{-3}])$^{-1}$ k_2: 8.6×10^{-6} d^{-1}
Root Mn^{2+} uptake	$Mn^{2+} \rightarrow$ Mn(uptake) + 2 H^+	Monod dependence on Mn^{2+} (k=0.1 μM), scaled by root biomass	1.7×10^{-7} mol L^{-1} d^{-1} (mmol root biomass C cm^{-3} soil)$^{-1}$

[1]Dwivedi, D., Arora, B., Steefel, C. I., Dafflon, B., & Versteeg, R. (2018). Hot Spots and Hot Moments of Nitrogen in a Riparian Corridor. *Water Resources Research*, *54*(1), 205–222. https://doi.org/10.1002/2017WR022346

References

Andre, B., Molins, S., Johnson, J., & Steefel, C. (2013). Alquimia. Berkeley, CA: Lawrence Berkeley National Laboratory.

Bandstra, J. Z., Ross, D. E., Brantley, S. L., & Burgos, W. D. (2011). Compendium and synthesis of bacterial manganese reduction rates. *Geochimica et Cosmochimica Acta, 75*(2), 337-351. doi:10.1016/j.gca.2010.04.069

Berg, B., Erhagen, B., Johansson, M.-B., Nilsson, M., Stendahl, J., Trum, F., & Vesterdal, L. (2015). Manganese in the litter fall-forest floor continuum of boreal and temperate pine and spruce forest ecosystems – A review. *Forest Ecology and Management, 358*, 248-260. doi:10.1016/j.foreco.2015.09.021

Berg, B., Erhagen, B., Johansson, M. B., Vesterdal, L., Faituri, M., Sanborn, P., & Nilsson, M. (2013). Manganese dynamics in decomposing needle and leaf litter—a synthesis. *Canadian Journal of Forest Research, 43*(12), 1127-1136.

Berg, B., Steffen, K. T., & McClaugherty, C. (2006). Litter decomposition rate is dependent on litter Mn concentrations. *Biogeochemistry, 82*(1), 29-39. doi:10.1007/s10533-006-9050-6

Bradford, M. A., Watts, B. W., & Davies, C. A. (2010). Thermal adaptation of heterotrophic soil respiration in laboratory microcosms. *Global Change Biology, 16*(5), 1576-1588. doi:https://doi.org/10.1111/j.1365-2486.2009.02040.x

Brantley, S. L., White, T., West, N., Williams, J. Z., Forsythe, B., Shapich, D., . . . Gu, X. (2018). Susquehanna Shale Hills Critical Zone Observatory: Shale Hills in the Context of Shaver's Creek Watershed. *Vadose Zone Journal, 17*(1). doi:10.2136/vzj2018.04.0092

Broadley, M., Brown, P., Cakmak, I., Rengel, Z., & Zhao, F. (2012). Function of nutrients: micronutrients. In *Marschner's mineral nutrition of higher plants* (pp. 191-248): Elsevier.

Chen, J., Luo, Y., van Groenigen, K. J., Hungate, B. A., Cao, J., Zhou, X., & Wang, R. W. (2018). A keystone microbial enzyme for nitrogen control of soil carbon storage. *Sci Adv, 4*(8), eaaq1689. doi:10.1126/sciadv.aaq1689

Ciais, P., Sabine, C., Bala, G., Bopp, L., Brovkin, V., Canadell, J., . . . Jones, C. (2013). *Carbon and other biogeochemical cycles. Climate change 2013: the physical science basis. Contribution of Working Group I to the Fifth Assessment Report of the Intergovernmental Panel on Climate Change.* Retrieved from

Conant, R. T., Ryan, M. G., Ågren, G. I., Birge, H. E., Davidson, E. A., Eliasson, P. E., . . . Bradford, M. A. (2011). Temperature and soil organic matter decomposition rates – synthesis of current knowledge and a way forward. *Global Change Biology, 17*(11), 3392-3404. doi:https://doi.org/10.1111/j.1365-2486.2011.02496.x

Davey, M. P., Berg, B., Emmett, B. A., & Rowland, P. (2007). Decomposition of oak leaf litter is related to initial litter Mn concentrations. *Canadian Journal of Botany, 85*(1), 16-24. doi:10.1139/b06-150

Doetterl, S., Stevens, A., Six, J., Merckx, R., Van Oost, K., Casanova Pinto, M., . . . Boeckx, P. (2015). Soil carbon storage controlled by interactions between geochemistry and climate. *Nature Geoscience, 8*(10), 780-783. doi:10.1038/ngeo2516

Dwivedi, D., Arora, B., Steefel, C. I., Dafflon, B., & Versteeg, R. (2018). Hot spots and hot moments of nitrogen in a riparian corridor. *Water Resources Research, 54*(1), 205-222.

Entwistle, E. M., Romanowicz, K. J., Argiroff, W. A., & Zak, D. (2019). Anthropogenic N Deposition Alters the Composition of Expressed Class II Fungal Peroxidases. *Appl Environ Microbiol, 84*, e02816-02817. doi:doi.org/10.1128/AEM .02816-17

Fernando, D. R., & Lynch, J. P. (2015). Manganese phytotoxicity: new light on an old problem. *Annals of botany, 116*(3), 313-319.

Frey, S. D., Ollinger, S., Nadelhoffer, K., Bowden, R., Brzostek, E., Burton, A., . . . Wickings, K. (2014). Chronic nitrogen additions suppress decomposition and sequester soil carbon in temperate forests. *Biogeochemistry, 121*(2), 305-316. doi:10.1007/s10533-014-0004-0

Fujii, K., Nakada, Y., Umezawa, K., Yoshida, M., Shibata, M., Hayakawa, C., . . . Hangs, R. (2020). A comparison of lignin-degrading enzyme activities in forest floor layers across a global climatic gradient. *Soil Ecology Letters, 2*(4), 281-294. doi:10.1007/s42832-020-0042-6

Fujii, K., Uemura, M., Hayakawa, C., Funakawa, S., & Kosaki, T. (2013). Environmental control of lignin peroxidase, manganese peroxidase, and laccase activities in forest floor layers in humid Asia. *Soil Biology and Biochemistry, 57*, 109-115. doi:10.1016/j.soilbio.2012.07.007

Garten, C. T., Wullschleger, S. D., & Classen, A. T. (2011). Review and model-based analysis of factors influencing soil carbon sequestration under hybrid poplar. *Biomass and Bioenergy, 35*(1), 214-226. doi:10.1016/j.biombioe.2010.08.013

Gonzalez, A., & Lynch, J. P. (1997). Effects of manganese toxicity on leaf CO2 assimilation of contrasting common bean genotypes. *Physiologia Plantarum, 101*(4), 872-880. doi:10.1111/j.1399-3054.1997.tb01076.x

Haaf, D., Six, J., & Doetterl, S. (2021). Global patterns of geo-ecological controls on the response of soil respiration to warming. *Nature Climate Change*. doi:10.1038/s41558-021-01068-9

Hammond, G. E., Lichtner, P. C., & Mills, R. T. (2014). Evaluating the performance of parallel subsurface simulators: An illustrative example with PFLOTRAN. *Water Resources Research, 50*(1), 208-228. doi:https://doi.org/10.1002/2012WR013483

Hancock, J. E., Loya, W. M., Giardina, C. P., Li, L., Chiang, V. L., & Pregitzer, K. S. (2007). Plant growth, biomass partitioning and soil carbon formation in response to altered lignin biosynthesis in Populus tremuloides. *New Phytol, 173*(4), 732-742. doi:10.1111/j.1469-8137.2006.01965.x

Hartley, I. P., Heinemeyer, A., & Ineson, P. (2007). Effects of three years of soil warming and shading on the rate of soil respiration: substrate availability and not thermal acclimation mediates observed response. *Global Change Biology, 13*(8), 1761-1770. doi:https://doi.org/10.1111/j.1365-2486.2007.01373.x

Hatakka, A., Lundell, T., Hofrichter, M., & Maijala, P. (2003). Manganese peroxidase and its role in the degradation of wood lignin. *In Applications of enzymes to lignocellulosics, American Chemical Society*, 230-243.

Haynes, R. (1990). Active ion uptake and maintenance of cation-anion balance: A critical examination of their role in regulating rhizosphere pH. *Plant and Soil, 126*(2), 247-264.

Herndon, E., Martínez, C. E., & Brantley, S. (2014). Spectroscopic (XANES/XRF) characterization of contaminant manganese cycling in a temperate watershed. *Biogeochemistry, 121*(3), 505-517. doi:10.1007/s10533-014-0018-7

Herndon, E. M., Jin, L., Andrews, D. M., Eissenstat, D. M., & Brantley, S. L. (2015). Importance of vegetation for manganese cycling in temperate forested watersheds. *Global Biogeochemical Cycles, 29*(2), 160-174. doi:10.1002/2014gb004858

Herndon, E. M., Martínez, C. E., & Brantley, S. L. (2014). Spectroscopic (XANES/XRF) characterization of contaminant manganese cycling in a temperate watershed. *Biogeochemistry, 121*(3), 505-517. doi:10.1007/s10533-014-0018-7

Hofrichter, M. (2002). Review: lignin conversion by manganese peroxidase (MnP). *Enzyme and Microbial Technology, 30*(4), 454-466. doi:10.1016/s0141-0229(01)00528-2

Hou, S. L., Hattenschwiler, S., Yang, J. J., Sistla, S., Wei, H. W., Zhang, Z. W., . . . Han, X. G. (2021). Increasing rates of long-term nitrogen deposition consistently increased litter decomposition in a semi-arid grassland. *New Phytol, 229*(1), 296-307. doi:10.1111/nph.16854

Huang, W., Yu, W., Yi, B., Raman, E., Yang, J., Hammel, K. E., . . . Hall, S. J. (2023). Contrasting geochemical and fungal controls on decomposition of lignin and soil carbon at continental scale. *Nat Commun, 14*(1), 2227. doi:10.1038/s41467-023-37862-6

Jin, L., Ravella, R., Ketchum, B., Bierman, P. R., Heaney, P., White, T., & Brantley, S. L. (2010). Mineral weathering and elemental transport during hillslope evolution at the Susquehanna/Shale Hills Critical Zone Observatory. *Geochimica et Cosmochimica Acta, 74*(13), 3669-3691. doi:10.1016/j.gca.2010.03.036

Jobbágy, E. J., & Jackson, R. B. (2004). The uplift of soil nutrients by plants: biogeochemical consequences across scales. *Ecology, 85*(9), 2380-2389.

Jones, M. E., LaCroix, R. E., Zeigler, J., Ying, S. C., Nico, P. S., & Keiluweit, M. (2020). Enzymes, Manganese, or Iron? Drivers of Oxidative Organic Matter Decomposition in Soils. *Environ Sci Technol, 54*(21), 14114-14123. doi:10.1021/acs.est.0c04212

Kabata-Pendias, A., & Pendias, H. (2001). *Trace elements in soils and plants* (3rd edition ed.): CRC Press.

Keiluweit, M., Nico, P., Harmon, M. E., Mao, J., Pett-Ridge, J., & Kleber, M. (2015). Long-term litter decomposition controlled by manganese redox cycling. *Proc Natl Acad Sci U S A, 112*(38), E5253-5260. doi:10.1073/pnas.1508945112

Kellner, H., Luis, P., Pecyna, M. J., Barbi, F., Kapturska, D., Krüger, D., . . . Hofrichter, M. (2014). Widespread occurrence of expressed fungal secretory peroxidases in forest soils. *PLoS One, 9*, e95557.

Kirschbaum, M. U. F. (2004). Soil respiration under prolonged soil warming: are rate reductions caused by acclimation or substrate loss? *Global Change Biology, 10*(11), 1870-1877. doi:https://doi.org/10.1111/j.1365-2486.2004.00852.x

Kogelmann, W. J., & Sharpe, W. E. (2006). Soil acidity and manganese in declining and nondeclining sugar maple stands in Pennsylvania. *J Environ Qual, 35*(2), 433-441. doi:10.2134/jeq2004.0347

Kramer, M. G., & Chadwick, O. A. (2018). Climate-driven thresholds in reactive mineral retention of soil carbon at the global scale. *Nature Climate Change, 8*(12), 1104-1108. doi:10.1038/s41558-018-0341-4

694 Kranabetter, J. M. (2019). Increasing soil carbon content with declining soil manganese in temperate rainforests: is
695 there a link to fungal Mn? *Soil Biology and Biochemistry, 128*, 179-181. doi:10.1016/j.soilbio.2018.11.001
696 Kranabetter, J. M., Philpott, T. J., & Dunn, D. E. (2021). Manganese limitations and the enhanced soil carbon
697 sequestration of temperate rainforests. *Biogeochemistry, 156*(2), 195-209. doi:10.1007/s10533-021-00840-
698 5
699 Lehmann, J., Hansel, C. M., Kaiser, C., Kleber, M., Maher, K., Manzoni, S., . . . Kögel-Knabner, I. (2020).
700 Persistence of soil organic carbon caused by functional complexity. *Nature Geoscience, 13*(8), 529-534.
701 doi:10.1038/s41561-020-0612-3
702 Li, H., Santos, F., Butler, K., & Herndon, E. (2021). A Critical Review on the Multiple Roles of Manganese in
703 Stabilizing and Destabilizing Soil Organic Matter. *Environ Sci Technol, 55*(18), 12136-12152.
704 doi:10.1021/acs.est.1c00299
705 Lichtner, P. C., Hammond, G. E., Lu, C., Karra, S., Bisht, G., Andre, B., . . . Kumar, J. (2015). *PFLOTRAN user*
706 *manual: A massively parallel reactive flow and transport model for describing surface and subsurface*
707 *processes*. Retrieved from
708 Luo, C., Rodriguez-R, L. M., Johnston, E. R., Wu, L., Cheng, L., Xue, K., . . . Konstantinidis, K. T. (2014). Soil
709 Microbial Community Responses to a Decade of Warming as Revealed by Comparative Metagenomics.
710 *Applied and Environmental Microbiology, 80*(5), 1777. doi:10.1128/AEM.03712-13
711 McCain, D. C., & Markley, J. L. (1989). More manganese accumulates in maple sun leaves than in shade leaves.
712 *Plant Physiology, 90*(4), 1417-1421.
713 Melillo, J. M., Frey, S. D., DeAngelis, K. M., Werner, W. J., Bernard, M. J., Bowles, F. P., . . . Grandy, A. S.
714 (2017). Long-term pattern and magnitude of soil carbon feedback to the climate system in a warming
715 world. *Science, 358*(6359), 101-105.
716 Moore, J. A. M., Anthony, M. A., Pec, G. J., Trocha, L. K., Trzebny, A., Geyer, K. M., . . . Frey, S. D. (2020).
717 Fungal community structure and function shifts with atmospheric nitrogen deposition. *Glob Chang Biol*.
718 doi:10.1111/gcb.15444
719 Morgenstern, I., Klopman, S., & Hibbett, D. S. (2008). Molecular evolution and diversity of lignin degrading heme
720 peroxidases in the Agaricomycetes. *J Mol Evol, 66*(3), 243-257. doi:10.1007/s00239-008-9079-3
721 Neupane, A., Herndon, E. M., Whitman, T., Faiia, A. M., & Jagadamma, S. (2023). Manganese effects on plant
722 residue decomposition and carbon distribution in soil fractions depend on soil nitrogen availability. *Soil*
723 *Biology and Biochemistry, 178*. doi:10.1016/j.soilbio.2023.108964
724 Oh, N.-H., & Richter, D. D. (2005). Elemental translocation and loss from three highly weathered soil–bedrock
725 profiles in the southeastern United States. *Geoderma, 126*(1-2), 5-25.
726 Parton, W. J., Hartman, M., Ojima, D., & Schimel, D. . (1998). DAYCENT and its land surface submodel:
727 description and testing. . *Global and Planetary Change, 19*(1-4), 35-48. doi:https://doi.org/10.1016/S0921-
728 8181(98)00040-X
729 Possinger, A. R., Heckman, K. A., Bowman, M. M., Gallo, A. C., Hatten, J. A., Matosziuk, L. M., . . . Strahm, B. D.
730 (2022). Lignin and fungal abundance modify manganese effects on soil organic carbon persistence at the
731 continental scale. *Geoderma, 425*. doi:10.1016/j.geoderma.2022.116070
732 Post, W. M., Izaurralde, R. C., Jastrow, J. D., McCarl, B. A., Amonette, J. E., Bailey, V. L., . . . Zhou, J. (2004).
733 Enhancement of Carbon Sequestration in US Soils. *BioScience, 54*(10), 895-908.
734 Remucal, C. K., & Ginder-Vogel, M. (2014). A critical review of the reactivity of manganese oxides with organic
735 contaminants. *Environ Sci Process Impacts, 16*(6), 1247-1266. doi:10.1039/c3em00703k
736 Ricciuto, D., Sargsyan, K., & Thornton, P. (2018). The Impact of Parametric Uncertainties on Biogeochemistry in
737 the E3SM Land Model. *Journal of Advances in Modeling Earth Systems, 10*(2), 297-319.
738 doi:https://doi.org/10.1002/2017MS000962
739 Richardson, J. B. (2017). Manganese and Mn/Ca ratios in soil and vegetation in forests across the northeastern US:
740 Insights on spatial Mn enrichment. *Sci Total Environ, 581-582*, 612-620.
741 doi:10.1016/j.scitotenv.2016.12.170
742 Romero-Olivares, A. L., Allison, S. D., & Treseder, K. K. (2017). Soil microbes and their response to experimental
743 warming over time: A meta-analysis of field studies. *Soil Biology and Biochemistry, 107*, 32-40.
744 doi:https://doi.org/10.1016/j.soilbio.2016.12.026
745 Santos, F., & Herndon, E. (2023). Plant-Soil Relationships Influence Observed Trends Between Manganese and
746 Carbon Across Biomes. *Global Biogeochemical Cycles, 37*(1). doi:10.1029/2022gb007412
747 Smith, D. B., Cannon, W. F., Woodruff, L. G., Solano, F., Kilburn, J. E., & Fey, D. L. (2013). *Geochemical and*
748 *mineralogical data for soils of the conterminous United States* (2327-638X). Retrieved from

749 Smith, L. A., Eissenstat, D. M., & Kaye, M. W. (2017). Variability in aboveground carbon driven by slope aspect
750 and curvature in an eastern deciduous forest, USA. *Canadian Journal of Forest Research, 47*(2), 149-158.
751 doi:10.1139/cjfr-2016-0147
752 St. Clair, S. B., & Lynch, J. P. (2004). Photosynthetic and antioxidant enzyme responses of sugar maple and red
753 maple seedlings to excess manganese in contrasting light environments. *Functional Plant Biology, 31*(10).
754 doi:10.1071/fp04049
755 St. Clair, S. B., & Lynch, J. P. (2005). Element accumulation patterns of deciduous and evergreen tree seedlings on
756 acid soils: implications for sensitivity to manganese toxicity. *Tree Physiology, 25*, 85-92.
757 Stendahl, J., Berg, B., & Lindahl, B. D. (2017). Manganese availability is negatively associated with carbon storage
758 in northern coniferous forest humus layers. *Sci Rep, 7*(1), 15487. doi:10.1038/s41598-017-15801-y
759 Stone, A. T., & Morgan, J. J. (1984). Reduction and Dissolution of Manganese(III) and Manganese(IV) Oxides by
760 Organics: 2. Survey of the Reactivity of Organics. *Environ Sci Technol, 18*, 617-624.
761 Sulman, B. N., Moore, J. A. M., Abramoff, R., Averill, C., Kivlin, S., Georgiou, K., . . . Classen, A. T. (2018).
762 Multiple models and experiments underscore large uncertainty in soil carbon dynamics. *Biogeochemistry,*
763 *141*(2), 109-123. doi:10.1007/s10533-018-0509-z
764 Sun, T., Cui, Y., Berg, B., Zhang, Q., Dong, L., Wu, Z., & Zhang, L. (2019). A test of manganese effects on
765 decomposition in forest and cropland sites. *Soil Biology and Biochemistry, 129*, 178-183.
766 doi:10.1016/j.soilbio.2018.11.018
767 Tebo, B. M., Bargar, J. R., Clement, B. G., Dick, G. J., Murray, K. J., Parker, D., . . . Webb, S. M. (2004). Biogenic
768 Manganese Oxides: Properties and Mechanisms of Formation. *Annual Review of Earth and Planetary*
769 *Sciences, 32*(1), 287-328. doi:10.1146/annurev.earth.32.101802.120213
770 Tian, Q., Liu, N., Bai, W., Li, L., Chen, J., Reich, P. B., . . . Zhang, W.-H. (2016). A novel soil manganese
771 mechanism drives plant species loss with increased nitrogen deposition in a temperate steppe. *Ecology,*
772 *97*(1), 65-74.
773 Todd-Brown, K. E. O., Randerson, J. T., Post, W. M., Hoffman, F. M., Tarnocai, C., Schuur, E. A. G., & Allison, S.
774 D. (2013). Causes of variation in soil carbon simulations from CMIP5 Earth system models and
775 comparison with observations. *Biogeosciences, 10*(3), 1717-1736. doi:10.5194/bg-10-1717-2013
776 Trum, F., Titeux, H., Cornelis, J.-T., & Delvaux, B. (2011). Effects of manganese addition on carbon release from
777 forest floor horizons. *Canadian Journal of Forest Research, 41*(3), 643-648. doi:10.1139/x10-224
778 Trum, F., Titeux, H., Ponette, Q., & Berg, B. (2015). Influence of manganese on decomposition of common beech
779 (Fagus sylvatica L.) leaf litter during field incubation. *Biogeochemistry, 125*(3), 349-358.
780 doi:10.1007/s10533-015-0129-9
781 Whalen, E. D., Smith, R. G., Grandy, A. S., & Frey, S. D. (2018). Manganese limitation as a mechanism for reduced
782 decomposition in soils under atmospheric nitrogen deposition. *Soil Biology and Biochemistry, 127*, 252-
783 263. doi:10.1016/j.soilbio.2018.09.025
784 Wieder, W. R., Allison, S. D., Davidson, E. A., Georgiou, K., Hararuk, O., He, Y., . . . Xu, X. (2015). Explicitly
785 representing soil microbial processes in Earth system models. *Global Biogeochemical Cycles, 29*(10),
786 1782-1800. doi:https://doi.org/10.1002/2015GB005188
787 Yi, B., Lu, C., Huang, W., Yu, W., Yang, J., Howe, A., . . . Hall, S. J. (2023). Resolving the influence of lignin on
788 soil organic matter decomposition with mechanistic models and continental-scale data. *Glob Chang Biol,*
789 *29*(20), 5968-5980. doi:10.1111/gcb.16875
790 Zaehle, S., Medlyn, B. E., De Kauwe, M. G., Walker, A. P., Dietze, M. C., Hickler, T., . . . Norby, R. J. (2014).
791 Evaluation of 11 terrestrial carbon–nitrogen cycle models against observations from two temperate Free-
792 Air CO2 Enrichment studies. *New Phytologist, 202*(3), 803-822. doi:https://doi.org/10.1111/nph.12697
793 Zak, D., Argiroff, W. A., Freedman, Z. B., Upchurch, R. A., Entwistle, E. M., & Romanowicz, K. J. (2019).
794 Anthropogenic N deposition, fungal gene expression, and an increasing soil carbon sink in the Northern
795 Hemisphere. *Ecology, 100*(10), e02804.
796